# Mapping the Local Density of Optical States of a Photonic Crystal with Single Quantum Dots

Qin Wang,[1,2] Søren Stobbe,[1,2] and Peter Lodahl[1,2]

[1]DTU Fotonik, Department of Photonics Engineering, Technical University of Denmark, Ørsteds Plads 343, DK-2800 Kongens Lyngby, Denmark

[2]Niels Bohr Institute, University of Copenhagen, Blegdamsvej 17, DK-2100 Copenhagen, Denmark

(Received 29 June 2011; published 12 October 2011)

We use single self-assembled InGaAs quantum dots as internal probes to map the local density of optical states of photonic crystal membranes. The employed technique separates contributions from nonradiative recombination and spin-flip processes by properly accounting for the role of the exciton fine structure. We observe inhibition factors as high as 70 and compare our results to local density of optical states calculations available from the literature, thereby establishing a quantitative understanding of photon emission in photonic crystal membranes.

DOI: 10.1103/PhysRevLett.107.167404 PACS numbers: 78.67.Pt, 42.50.Ct, 78.47.D−, 78.67.Hc

Photonic crystals (PCs) are artificial periodic dielectric materials that were originally proposed as a way to control the dynamics of spontaneous emission of light potentially leading to efficient light sources and solar cells [1]. Embedding light sources inside photonic crystals has enabled the experimental demonstration of modified spontaneous emission using dye molecules [2,3], quantum wells [4], or quantum dots [5–9]. The complexity of light-matter interaction in PCs is apparent since the experiments combine inhomogeneous dielectric materials varying on the scale of the wavelength with inherently mesoscopic quantum emitters. Within the validity of the dipole approximation, which is valid for standard-sized quantum dots in dielectric structures [10], the light-matter coupling is determined by two quantities: (i) the transition dipole moment of the optical transition and (ii) the local density of optical states (LDOS) projected onto the orientation of the dipole [11,12]. The latter is a property of the PC that accounts for all available Bloch modes at a specific position and has been exceedingly challenging to calculate in realistic structures relevant for experiments [11,13]. Consequently, a thorough understanding of the LDOS and therefore the potential of spontaneous emission control has been lacking in PCs. Here we present the experimental mapping of the LDOS of PCs by time-resolved emission studies of single quantum dots (QDs) with well-characterized optical properties.

The focus of the present work is to use QDs as internal probes of the LDOS. This quest requires a detailed understanding of the optical properties of QDs in inhomogeneous media and, in particular, the role of the exciton fine structure. Our previous work on dielectric interfaces demonstrated the necessity to consider the role of dark excitons [14] and proved the validity of the dipole approximation for standard-sized QDs in dielectric structures [10], while a breakdown of the dipole approximation was observed near metallic interfaces [15]. Building on this knowledge, we present a new and general method to extract the *radiative* decay rate of single QDs as opposed to the *total* decay rate that is otherwise directly measured in time-resolved spectroscopy and is significantly influenced by dark excitons and nonradiative decay processes. From the radiative decay rate, we determine the LDOS and experimentally map it by recording decay curves of many single QDs positioned throughout the 2D PC membranes. We compare our results with LDOS simulations performed with 3D finite-difference time-domain simulations available in the literature [13] and explicitly demonstrate the importance of extracting the radiative decay rate. We observe record high spontaneous emission inhibition factors of 70 compared to QDs in homogenous media, which proves the potential of 2D PC membranes for applications where spontaneous emission is a nuisance. The frequency dependency of the LDOS is mapped out both inside and outside the 2D band gap, and in the latter case also enhancement of the spontaneous emission rate is observed.

Within the dipole approximation and for weak light-matter interaction strengths, the radiative decay rate is directly proportional to the LDOS: $\gamma_{\mathrm{rad}}(\mathbf{r_0}, \omega) = \frac{\pi\omega}{3\hbar\varepsilon_0}|\boldsymbol{\mu}|^2\rho_\mu(\mathbf{r_0}, \omega)$, where $\rho_\mu(\mathbf{r_0}, \omega)$ is the projected LDOS evaluated at the position $\mathbf{r_0}$ and emission frequency $\omega$ of the emitter, $\varepsilon_0$ is the vacuum permittivity, and $\boldsymbol{\mu}$ is the transition dipole moment. The LDOS describes the electromagnetic environment and can be calculated from the dyadic Green's function [16]. Successfully extracting the radiative decay rate provides a mean of obtaining the LDOS by comparing to the radiative decay rate in a homogeneous medium $\gamma_{\mathrm{rad}}^{\mathrm{hom}}(\omega)$ using the relation

$$\rho_\mu(\mathbf{r_0}, \omega) = \frac{\gamma_{\mathrm{rad}}(\mathbf{r_0}, \omega)}{\gamma_{\mathrm{rad}}^{\mathrm{hom}}(\omega)}\rho(\omega), \tag{1}$$

where $\rho(\omega) = \frac{n\omega^2}{3\pi^2c^3}$ is the projected LDOS for a homogeneous medium with refractive index $n$ and $c$ is the speed of light in vacuum.

 

A detailed understanding of the exciton fine structure and the role of nonradiative recombination is required in order to use QDs as LDOS probes [10,14,17]. An InGaAs QD has two optically active bright states with total angular momentum $J_z = \pm 1$ and two dark states with $J_z = \pm 2$, where the quantization axis $z$ is the growth direction [001] [18]. Because of the reduced symmetry and anisotropic exchange interactions, the two bright states are separated in energy and form two eigenstates $X$ and $Y$ named according to their dipole orientations ([110] or $[1\bar{1}0]$), where $|X\rangle_b = (|+1\rangle + |-1\rangle)/\sqrt{2}$ and $|Y\rangle_b = (|+1\rangle - |-1\rangle)/\sqrt{2}$. Similarly, the two dark states are separated into $|X\rangle_d = (|+2\rangle + |-2\rangle)/\sqrt{2}$ and $|Y\rangle_d = (|+2\rangle - |-2\rangle)/\sqrt{2}$. The PC patterns can be aligned relative to $X$ and $Y$, as schematically indicated in Fig. 1(a).

The two bright and two dark states together with the ground state form a five-level model. $|X\rangle_b$ couples to $|X\rangle_d$ through either an electron or a hole spin flip mediated by phonons and exchange interaction [19]. We note that spin-flip processes coupling bright excitons, i.e., $|X\rangle_b \leftrightarrows |Y\rangle_b$, are slow compared to the other decay processes and therefore can be abandoned in the analysis, as theoretically predicted [19,20] and experimentally confirmed from the large anisotropy in the decay rate for $X$ and $Y$ states observed in a PC [21]. Consequently, the five-level scheme can be simplified to the three-level system indicated in Fig. 1(c). The bright state can decay through either radiative or nonradiative processes with rates $\gamma^{X,b}_{\mathrm{rad}}$ and $\gamma^{X,b}_{\mathrm{nrad}}$, respectively, and is coupled to the dark state through a spin-flip rate $\gamma^{X}_{bd}$. Radiative transitions from the dark state to the ground state are forbidden, but nonradiative recombination is possible with the rate $\gamma^{X,d}_{\mathrm{nrad}}$ together with spin flips to the bright state with a rate $\gamma^{X}_{db}$. Solving the resulting rate equations, we find that the population of bright excitons decay biexponentially: $\rho^X_b(t) = A_f e^{-\gamma^X_f t} + A_s e^{-\gamma^X_s t}$, with $\gamma^X_f = \gamma^{X,b}_{\mathrm{nrad}} + \frac{1}{2}\gamma^{X,b}_{\mathrm{rad}} + \gamma^X_{db} + \sqrt{(\gamma^X_{db})^2 + (\gamma^{X,b}_{\mathrm{rad}}/2)^2}$, $\gamma^X_s = \gamma^{X,b}_{\mathrm{nrad}} + \frac{1}{2}\gamma^{X,b}_{\mathrm{rad}} + \gamma^X_{db} - \sqrt{(\gamma^X_{db})^2 + (\gamma^{X,b}_{\mathrm{rad}}/2)^2}$, $A^X_f = \frac{\rho^X_b(0)}{2}[1 + \frac{\gamma^{X,b}_{\mathrm{rad}}}{\gamma^X_f - \gamma^X_s}] - \rho^X_d(0)\frac{\gamma^X_{db}}{\gamma^X_f - \gamma^X_s}$, and $A^X_s = \frac{\rho^X_b(0)}{2}[1 - \frac{\gamma^{X,b}_{\mathrm{rad}}}{\gamma^X_f - \gamma^X_s}] + \rho^X_d(0)\frac{\gamma^X_{db}}{\gamma^X_f - \gamma^X_s}$. Similar expressions can be obtained for $\rho^Y_b(t)$. $\rho^X_b(0)$ and $\rho^X_d(0)$ are the initial populations of the bright and dark states, respectively. For nonresonant and weak pumping, we have $\rho^X_d(0) = \rho^X_b(0) = 0.5$, where we note that the presented results of the LDOS mapping are robust to deviations from this equilibrium condition. Furthermore, we have assumed (i) $\gamma^X_{bd} = \gamma^X_{db}$ and (ii) $\gamma^{X,b}_{\mathrm{nrad}} = \gamma^{X,d}_{\mathrm{nrad}}$. (i) is a good approximation for intermediate temperatures ($T = 10$ K in our experiment), because $\gamma_{bd} = e^{\delta_{bd}/k_B T}\gamma_{db}$, and $k_B T \gg \delta_{bd}$, where $k_B$ is the Boltzmann constant and $\delta_{bd}$ is the energy splitting between the bright and dark states (typically, a few hundred $\mu$eV [18]). Assumption (ii) has been proven valid by

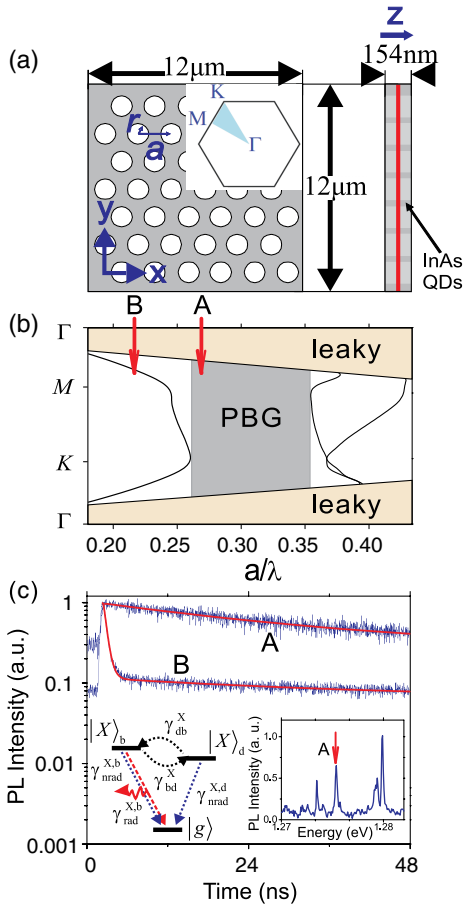


FIG. 1 (color online). (a) Sketch of a PC membrane, top view (left) and side view (right). The orientations of the $X$ and $Y$ dipoles together with the sample growth direction ($Z$) are schematically indicated. The inset shows the first Brillouin zone with indications of the relevant symmetry directions. (b) A photonic-band diagram calculated for optical modes with in-plane polarization, where the gray region represents the 2D photonic-band gap (PBG) and "leaky" refers to the regions where light is not confined to the membrane. (c) Measured decay curves of QDs $A$ and $B$ that are, respectively, tuned in- or outside the band gap, as schematically indicated in (b). The insets show the three-level diagram of the QD (left) and a measured emission spectrum (right).

experiments on QDs in dielectric media with a known LDOS [14,17]. The intensity measured in a time-resolved experiment is $I^X(t) = C_0\gamma^{X,b}_{\mathrm{rad}}\rho^X_b(t)$, where $C_0$ is proportional to the total collection efficiency of the experimental setup, which is an overall scaling factor of the decay curves. After fitting each decay curve with a biexponential function, we obtain the three parameters $\gamma^i_f$, $\gamma^i_s$, and $A^i_f/A^s_f$ (for $i = X, Y$), and $\gamma^i_{\mathrm{rad}}$, $\gamma^i_{\mathrm{nrad}}$, and $\gamma^i_{bd}$ can be extracted from the relations described above. The amplitudes need to be corrected to account for residual population of the QD when it is reexcited by a light pulse [14]: $A^i_f = \tilde{A}^i_f[1 - \exp(-\gamma^i_f\tau)]$ and $A^i_s = \tilde{A}^i_s[1 - \exp(-\gamma^i_s\tau)]$, where $\tau$ is the excitation period and $\tilde{A}^i_f$ ($\tilde{A}^i_s$) refers to the measured

amplitude. We stress that the presented method is completely general; i.e., no assumptions about the magnitude of the rates have been implemented, and therefore InGaAs QDs can be employed as LDOS probes in any nanophotonic environment.

We have carried out time-resolved measurements on single self-assembled QDs positioned in- or outside 2D PC membranes. The experiments are done in a flow cryostat at 10 K, and the sample consists of a series of 2D GaAs ($n = 3.5$) PC membranes with a layer of InGaAs QDs (density $\sim 80\ \mu m^{-2}$) embedded in the center. The dimension of each PC membrane is $12 \times 12\ \mu m^2$ with a thickness of 154 nm as shown in Fig. 1(a), where also the orientations of $X$ and $Y$ dipoles are indicated. Figure 1(b) shows the photonic-band diagram of the structure with indications of the 2D photonic-band gap region and the continuum due to coupling to leaky modes out of the membrane. The lattice parameter ($a$) ranges from 200 to 385 nm in steps of 5 nm, and the $r/a$ ratio is fixed at 0.30, where $r$ is the radius of the air hole. The QDs are excited with a PicoQuant PDL-800 pulsed diode laser at 781 nm with a varying repetition rate (5, 10, 20, and 40 MHz). Under weak excitation conditions, we identify neutral excitons by their excitation power and polarization dependence; i.e., multiexciton complexes are excluded due to the observed linear power dependence before saturation, while single-charge excitons are found to be monoexponential and have a very weak polarization dependence. We select only QDs that emit within a narrow spectral range of $970 \pm 5$ nm, in order to probe QDs with similar oscillator strengths [10], while different scaled frequencies are accessed by varying $a$. In total, 88 QDs in the PC are probed, in addition to 5 QDs positioned outside the PC pattern, that serve as a reference. For each QD, a polarizer is used to record emission from either the $X$ or the $Y$ exciton state.

Figure 1(c) shows two typical decay curves of QD $A$ and $B$ ($X$ states) that are tuned, respectively, in- or outside the band gap. Clearly, the decay of QD $A$ is strongly suppressed as a consequence of the strongly suppressed LDOS associated with the 2D band gap of the structure. QD $B$ is positioned in a PC that is designed to probe the LDOS at the edge of the band gap, and indeed a much faster decay is observed in this case. Based on the method explained above, we can extract the radiative decay rate of each exciton state and obtain the projected LDOS. The results are shown in Fig. 2 including a comparison to the theory of Koenderink *et al.* [13], who calculated the projected LDOS for 7 specific positions in a PC membrane. Also shown is the density of optical states for a homogeneous medium (dash-dotted line). In order to compensate for a slight difference in membrane thickness between the experiment and theory, we have extended the band gap width according to the theory of Ref. [22]. We observe a pronounced 2D band gap leading to a wide range of frequencies where the LDOS is strongly suppressed for

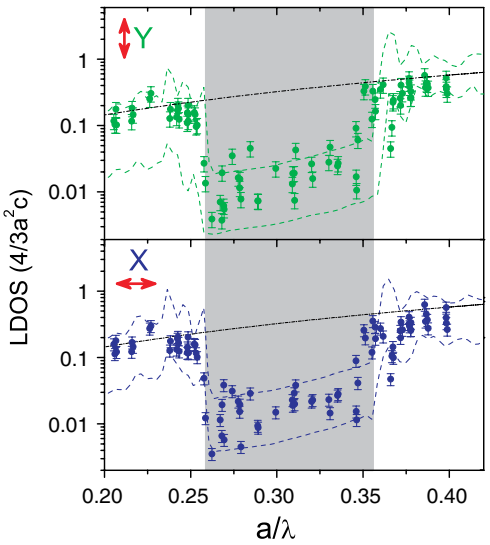


FIG. 2 (color online). Measured projected LDOS of PC membranes versus scaled emission frequencies for $X$ and $Y$ dipole orientations (data points). The two dashed lines represent the maximum and minimum values of the calculated projected LDOS as taken from Ref. [13]. For reference, also the density of optical states of homogeneous GaAs is indicated (black dash-dotted lines), and the gray areas represent the band gap.

both $X$ and $Y$ exciton states. Large point-to-point fluctuations in the experimental data are observed, since the QDs exhibit different radiative decay rates due to their varying positions in the PC membrane, thus reflecting the sensitive spatial variation of the LDOS. Outside the band gap, an enhanced LDOS is observed at some frequencies relative to the density of optical states of a homogeneous medium. Consequently, the decay rate of QDs tuned to the band edge can be Purcell enhanced in this case by coupling to extended Bloch modes as opposed to localized cavity modes, which is the most common way of realizing the Purcell effect. In general, good agreement between the experiment and theory is observed, especially taking into consideration that the spatial sampling used in the theory is rather sparse, while in the experiment the QDs occupy all different positions in the high refractive index material. Interestingly, the experimental data appear to be biased such that the measured LDOS seems systematically larger than predicted by theory, in particular, for normalized frequencies below the 2D band gap. This observation is likely an effect of unavoidable fabrication imperfections that would be more severe for the small feature sizes corresponding to reduced frequencies below the band gap. Such disorder has been found to lead to significant modifications of the LDOS in PC waveguides [23], and it is therefore important to quantify the role of disorder in any PC application, which is done here through the comparison with theory. Furthermore, we note that the actual size of our sample is larger than that used in the simulations, which will diminish the Fabry-Perot oscillations observed below the band gap.

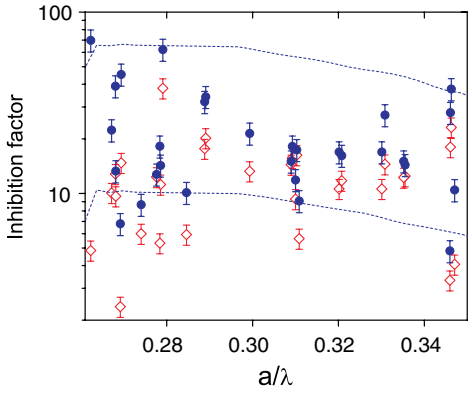


FIG. 3 (color online). Inhibition factors for QDs inside the 2D photonic-band gap. The blue circular points are obtained from the full model accounting for the exciton fine structure and nonradiative recombination, while the red diamond points are obtained by incorrectly using directly measured total decay rates. The two dashed blue lines show the maximum and minimum values from simulations [13].

For reference, we have also measured the radiative decay rate, nonradiative decay rate, and spin-flip rate of 5 QDs positioned outside the PC area and obtain the average values $\gamma^i_{\mathrm{rad}} = 1.1 \pm 0.1\ \mathrm{ns}^{-1}$, $\gamma^i_{\mathrm{nrad}} = 0.06 \pm 0.05\ \mathrm{ns}^{-1}$, and $\gamma^i_{bd} = 0.005 \pm 0.002\ \mathrm{ns}^{-1}$, respectively, from which we extract the average radiative decay rate of QDs in a homogeneous medium of $\gamma^{\mathrm{hom}}_{\mathrm{rad}} = 1.3 \pm 0.1\ \mathrm{ns}^{-1}$ by calculating the LDOS of the QDs positioned 77 nm from the GaAs-air interface. The corresponding quantum efficiency is 95% ± 13%, and both numbers agree well with previous results [10,14,17]. Focusing on QDs positioned in the band gap, we extract the inhibition factor relative to this reference value in the homogenous medium; see Fig. 3. A maximum inhibition factor of 70 is observed, which is to our knowledge the highest value ever reported in any PC. We stress the necessity of employing the presented method that accounts for the QD fine structure and nonradiative recombination in order to correctly extract the inhibition factors. Thus, Fig. 3 also displays the inhibition factors derived by using the common but incorrect assumption that the directly measured total decay rate is dominated by radiative recombination. The large dot-to-dot fluctuations reflect the sensitivity of spin-flip and nonradiative processes to inhomogeneities. This comparison clearly illustrates the importance of employing the correct microscopic model of the quantum emitter in order to use them as LDOS probes.

In conclusion, we have presented a method to probe the LDOS of any nanoenvironment by employing self-assembled InGaAs QDs. By properly accounting for the exciton fine structure, it is possible to extract the radiative decay rate and therefore eliminate effects from nonradiative recombination and spin-flip processes. We presented a detailed frequency map of the LDOS and a detailed comparison to existing theory. Inhibition factors as high as 70 were observed inside the 2D band gap, thus clearly demonstrating the potential of PC membranes for efficient spontaneous emission inhibition. Our work is expected to lay the foundation for further exploitations of photonic crystal membranes for all-solid-state quantum electrodynamics experiments, where the LDOS is the essential quantity that controls not only spontaneous emission but also, e.g., the Lamb shift [24] or Casimir forces.

The authors thank P. T. Kristensen, H. T. Nielsen for useful discussions, and A. F. Koenderink for generously sharing the data of his LDOS simulations. We gratefully acknowledge financial support from the Villum Foundation, The Danish Council for Independent Research (Natural Sciences and Technology and Production Sciences), and the European Research Council (ERC consolidator grant).

[1] E. Yablonovitch, Phys. Rev. Lett. **58**, 2059 (1987).
[2] A. F. Koenderink, L. Bechger, H. P. Schriemer, A. Lagendijk, and W. L. Vos, Phys. Rev. Lett. **88**, 143903 (2002).
[3] I. S. Nikolaev, P. Lodahl, and W. L. Vos, J. Phys. Chem. C **112**, 7250 (2008).
[4] M. Fujita *et al.*, Science **308**, 1296 (2005).
[5] P. Lodahl *et al.*, Nature (London) **430**, 654 (2004).
[6] M. Kaniber *et al.*, Phys. Rev. B **77**, 073312 (2008).
[7] B. Julsgaard *et al.*, Appl. Phys. Lett. **93**, 094102 (2008).
[8] I. S. Nikolaev, P. Lodahl, A. F. van Driel, A. F. Koenderink, and W. L. Vos, Phys. Rev. B **75**, 115302 (2007).
[9] S. Noda, M. Fujita, and T. Asano, Nat. Photon. **1**, 449 (2007).
[10] J. Johansen *et al.*, Phys. Rev. B **77**, 073303 (2008).
[11] K. Busch and S. John, Phys. Rev. E **58**, 3896 (1998).
[12] R. Sprik, B. A. V. Tiggelen, and A. Lagendijk, Europhys. Lett. **35**, 265 (1996).
[13] A. F. Koenderink, M. Kafesaki, C. M. Soukoulis, and V. Sandoghdar, J. Opt. Soc. Am. B **23**, 1196 (2006).
[14] J. Johansen, B. Julsgaard, S. Stobbe, J. M. Hvam, and P. Lodahl, Phys. Rev. B **81**, 081304(R) (2010).
[15] M. L. Andersen, S. Stobbe, A. S. Sørensen, and P. Lodahl, Nature Phys. **7**, 215 (2011).
[16] L. Novotny and B. Hecht, *Principles of Nano-Optics* (Cambridge University Press, Cambridge, England, 2006).
[17] S. Stobbe, J. Johansen, P. T. Kristensen, J. M. Hvam, and P. Lodahl, Phys. Rev. B **80**, 155307 (2009).
[18] M. Bayer *et al.*, Phys. Rev. B **65**, 195315 (2002).
[19] K. Roszak, V. M. Axt, T. Kuhn, and P. Machnikowski, Phys. Rev. B **76**, 195324 (2007); **77**, 249905(E) (2008).
[20] E. Tsitsishvili and H. Kalt, Phys. Rev. B **82**, 195315 (2010).
[21] Q. Wang *et al.*, Opt. Lett. **35**, 2768 (2010).
[22] L. C. Andreani and M. Agio, IEEE J. Quantum Electron. **38**, 891 (2002).
[23] L. Sapienza, H. Thyrrestrup, S. Stobbe, P. D. Garcia, S. Smolka, and P. Lodahl, Science **327**, 1352 (2010).
[24] N. Vats, S. John, and K. Busch, Phys. Rev. A **65**, 043808 (2002).